Applied Catalysis A, General 580 (2019) 53–58

Contents lists available at ScienceDirect

Applied Catalysis A, General

journal homepage: www.elsevier.com/locate/apcata

Effects of WO_3 nanoparticle size on ethylene-butene metathesis activity

Shiran Zhang[a], Daniel F. Consoli[a], Sohel K. Shaikh[b], Yuriy Román-Leshkov[a,*]

[a] Department of Chemical Engineering, Massachusetts Institute of Technology, 77 Massachusetts Avenue, Cambridge, MA, 02139, United States
[b] Research and Development Center, Saudi Aramco, Dhahran, 31311, Saudi Arabia

ARTICLE INFO

Keywords:
Metathesis
Tungsten oxide
Size effect
Ethylene
Butene

ABSTRACT

WO_3 nanoparticles (NPs) of 2.64 ± 1.11 nm, 16.6 ± 3.7 nm, and 54.3 ± 18.5 nm were investigated in the cross-metathesis reaction of ethylene and trans-2-butene to form propylene. Measurements of reaction rates normalized by exposed WO_3 surface area showed that decreasing WO_3 particle sizes resulted in increasing propylene formation rates. X-ray photoelectron spectroscopy of post-reaction catalysts showed that smaller WO_3 NPs featured lower O/W surface atomic ratios, and thus higher degrees of surface unsaturation. Based on these results, high-temperature synthetic treatments aimed at increasing the degree of surface unsaturation of WO_3 NPs showed significant improvements in metathesis activity when compared to baseline values. This work demonstrates that control of particle size for industrially-relevant catalysts drastically impacts reactivity.

1. Introduction

Due to the growing demand of propylene globally, the cross-metathesis of ethylene and 2-butene to propylene has received renewed interest as it provides a feasible avenue for large-scale propylene production [1–3]. The most common heterogeneous catalysts for this reaction include Re_2O_7, MoO_3, and WO_3 nanoparticles supported on silica or alumina. While supported Re_2O_7 and MoO_3 are able to catalyze the cross-metathesis at lower temperatures, the supported WO_3 catalyst continues to be attractive by virtue of its low cost, high robustness, and tolerance to trace amount of oxygenates [1]. Consequently, extensive research efforts have been dedicated to the investigation and optimization of WO_3/SiO_2 catalysts both experimentally and theoretically to identify the nature of active sites [4,5], the effects of catalyst support [6–9] and W loading [10,11], the intrinsic reaction kinetics [12,13], as well as the various catalyst activation/deactivation processes [14–17]. However, the effects of WO_3 particle size on catalytic performance have not been investigated in a systematic fashion.

Indeed, industrial catalysts usually possess a wide distribution of particle sizes [1]. The measured catalytic performance represents an average of the various contributions from all the sites present in NPs with different sizes and surface structures [18]. In order to improve performance, it is of practical significance to understand the effects of particle size on metathesis activity and selectivity. The surface of the WO_3 NP mainly consists of terraces, step edges, and corners, where W atoms at these locations have different coordination environments. W atoms at terraces are generally more saturated than those at step edges and corners. Compared with highly-coordinated oxygen atoms at terraces, those at edges and corners are more prone to form vacancies (i.e., unsaturated sites). Such differences in coordination environment impact the oxidation state of W and the geometry of the surface sites, both of which mediate the adsorption energy of olefin molecules and/or reaction intermediates, ultimately leading to different catalytic performance [19]. More importantly, the surface composition of these surface structures changes as a function of particle size, with a decrease in particle size favoring step edges and corners at the expense of terrace sites [20].

In this study, the size effect of WO_3 NPs on the metathesis activity of the cross-metathesis of ethylene and trans-2-butene to form propylene was investigated. In order to minimize support effects, the NPs were used in the absence of a support or were supported on inert graphite, given that oxide supports, such as SiO_2 and Al_2O_3 have been shown to influence the metathesis activity of WO_x [1]. The metathesis activity showed a strong dependence on particle size when comparing propylene production rates normalized by surface area. Characterization studies revealed that this size dependence was related to the degree of surface unsaturation.

2. Experimental Section

2.1. Catalyst synthesis

Small-sized WO_3 NPs were prepared by a reverse microemulsion (RME) protocol at room temperature described in literature [21]. In a

* Corresponding author.
E-mail address: yroman@mit.edu (Y. Román-Leshkov).

https://doi.org/10.1016/j.apcata.2019.04.019
Received 30 January 2019; Received in revised form 12 April 2019; Accepted 16 April 2019
Available online 27 April 2019
0926-860X/

typical synthesis, 8.8 ml of Igepal CO-520 surfactant (Sigma Aldrich, used as received) was mixed in 50 ml of n-heptane (Sigma Aldrich, 99%, used as received) followed by 1.1 ml of 0.2 M HCl aqueous solution to form a clear and colorless solution, termed Solution I. In another setup, 8.8 ml of Igepal CO-520 were mixed in 50 ml of n-heptane followed by 1.1 ml of 0.2 M Na_2WO_4 aqueous solution to form a clear and colorless solution, termed Solution II. Next, Solution II was transferred to Solution I by way of a syringe in 30 min, and the mixture was stirred for 8 h. After that, 30 ml of methanol (Sigma Aldrich, used as received) was added to break the reverse microemulsion by forming a two-phase system. After decanting the heptane phase, white precipitate was collected by centrifugation of the alcohol phase and re-dispersed in 30 ml of methanol. Then 0.5 g of graphite powder (Sigma Aldrich, 99.99% trace metals basis, used as received) powder was added and the mixture was loaded onto a rotovap. After the vaporization of methanol at 40 °C, the remaining solid was collected and calcined in air at 350 °C for 3 h to obtain 1 wt% small-sized WO_3 NPs/graphite, termed 1% s-WO_3 NPs/graphite. The small-sized WO_3 NPs on the graphite support were termed s-WO_3 NPs. Note that graphite does not undergo thermal degradation at this temperature, as confirmed by thermogravimetric analysis of the bare support [22]. The small nanoparticles were supported in graphite in order to avoid agglomeration and fully expose their surface area.

Medium-sized WO_3 NPs were prepared with a modified hydrothermal protocol described in literature [23]. Briefly, 0.99 g of $Na_2WO_4{\cdot}2H_2O$ (Sigma Aldrich, > 99%, used as received) was dissolved in 20 ml of deionized water and 2 M HCl was added into the solution dropwise forming a yellow precipitate. The precipitate was collected by centrifugation and re-dissolved in 40 ml of 1 M oxalic acid solution. After that, 4.37 g of cetyltrimethyl ammonium bromide (CTAB) (Sigma Aldrich, used as received) was added to the solution, which was then transferred into a 50 ml Teflon-lined stainless steel autoclave. The mixture was then heated at 180 °C for 12 h, and cooled down to room temperature. The solids were collected by centrifugation, dried at 100 °C overnight, followed by calcination in air at 350 °C for 3 h. The final product is termed m-WO_3 NPs.

Large-sized WO_3 NPs (Sigma Aldrich, nanopowder, < 100 nm, used as received), were purchased, and calcined in air at 350 °C for 3 h before use. This material is termed lg-WO_3 NPs.

2.2. Catalyst characterization

The size and morphology of WO_3 NPs were characterized using an FEI Tecnai Multipurpose transmission electron microscope (TEM) operated at an accelerating voltage of 120 kV. TEM images were analyzed by Digital Micrograph (Gatan) software. Powder X-ray diffraction (PXRD) patterns of l-WO_3 NPs and m-WO_3 NPs were recorded with a Bruker D8 X-ray diffractometer using Cu Kα radiation (λ = 1.54056 Å) operated at 40 kV and 40 mA in a continuous mode in the 2θ range from 20° to 60°. Surface areas of lg-WO_3 NPs and m-WO_3 NPs were measured on a Quantachrome AutosorbiQ automated gas sorption analyzer using low temperature N_2 adsorption. The loading percentage of 1% s-WO_3 NPs/graphite was confirmed by inductively coupled plasma-optical emission spectrometry (ICP-OES) (Agilent ICP-OES VDV 5100).

X-ray photoelectron spectroscopy (XPS) was performed using a PHI VersaProbe II X-ray photoelectron spectrometer with monochromated Al Kα X-ray source. Air-free measurements were performed by loading post-reaction catalysts into a transfer vessel in the glove box, which could be attached to the XPS without exposure to air. A dual-beam charge neutralizer was applied to compensate for the charging effect. The acquired spectra were calibrated with C 1 s peak at 284.5 eV, and analyzed using CasaXPS software. The spectra fitting follows the peak positions reported in literature [24]. All fitted components have the same Full-Width-Half-Maximum (FWHM), and identical fitting parameters were applied to all spectra.

2.3. Reactivity tests

Reactivity tests of the as-prepared catalysts were carried out in a ¼" stainless steel reactor within an insulated single-zone furnace (Applied Test Systems series 3210, 850 W/115 V). 200 mg of a catalyst sample (pelletized into 40–60 mesh size) was packed in between two quartz wool plugs and two sets of 100 mg of SiC (46 grit, Alfa Aesar, used as received). Reaction temperatures were monitored and maintained by a K-type thermocouple (Omega Engineering), placed underneath the catalyst bed, and a PID temperature controller (Cole Parmer Digi-Sense 89000 series). All gases were delivered via calibrated mass flow controllers (Brooks Instrument SLA 5800 series) and purified through a trap containing Q5 copper catalyst (Research Catalysts, Inc.) and 3 A molecular sieves (Sigma Aldrich) to remove oxygen and moisture, respectively, before entering the reactor tube. The catalyst was pretreated in He (100 ml/min) at 550 °C for 1 h, and then cooled down to the reaction temperature of 350 °C in He. All pretreatments and reaction conditions were kept at atmospheric pressure. The reactant gas mixture consisted of equimolar 10% ethylene and 10% trans-2-butene balanced with He, introduced at a rate of 100 ml/min. Effluent gases were analyzed with an on-line gas chromatograph (Shimadzu GC-2014) equipped with an Agilent HP-PLOT Al_2O_3-S (30 m × 0.25 mm) column and a flame ionization detector (FID) for the analysis of both the reactants and products. All catalytic studies were measured in terms of the formation rates of propylene for metathesis in the kinetically controlled regime and in the absence of mass transfer limitations, which was verified using different flow rates and catalyst particle sizes. The mass balance closure was kept above 99%.

3. Results and discussion

3.1. Characterization of WO_3 NPs before reaction

As shown in Fig. 1, the average sizes of large-, medium- and small-sized WO_3 NPs were 54.3 ± 18.5 nm, 16.6 ± 3.7 nm, and 2.64 ± 1.11 nm, respectively, as obtained by a Gaussian fitting of the size distribution measured from TEM images. The nanoparticles of 1% s-WO_3 NPs/graphite have a wider size distribution relative to the size of lg-WO_3 NPs and m-WO_3 NPs due to the challenge in controlling ultra-small sizes within a very narrow distribution. Fig. 2 presents the diffraction patterns of lg-WO_3 NPs and m-WO_3 NPs that are consistent with hexagonal WO_3 (PDF No. 43-1035). Due to the small size and low loading of WO_3 NPs in 1% s-WO_3 NPs/graphite, the diffraction pattern did not contain any features associated with crystalline WO_3. We therefore worked under the assumption that small-sized WO_3 NPs would have a similar crystallographic structure to that of the lg- and m-WO_3 NPs, since identical calcination conditions were used.

Table 1 lists the surface areas of different-sized WO_3 NPs calculated both from average particle size in TEM and from N_2 adsorption using the Brunauer-Emmett-Teller (BET) method (except for s-WO_3). Both techniques showed comparable surface areas for lg-WO_3 NPs and m-WO_3 NPs. Therefore, TEM surface areas were used for subsequent normalization of reaction rates.

3.2. Catalytic performances of different-sized WO_3 NPs in ethylene and trans-2-butene cross-metathesis

Propylene was produced from the cross-metathesis of ethylene and trans-2-butene at 350 °C over WO_3 NPs. As shown in Fig. 3a, lg-WO_3 NPs, m-WO_3 NPs, and 1% s-WO_3 NPs/graphite yield specific propylene formation rates of 2.5×10^{-3}, 5.4×10^{-2}, and 3.4 mmol/g/h, respectively, which, while lower than metathesis rates typically obtained in industry using supported catalysts, are consistent with the metathesis activities reported for bulk WO_3 [25]. In order to eliminate the potential differences caused by differences in surface areas, the propylene formation rates were instead normalized by the respective calculated

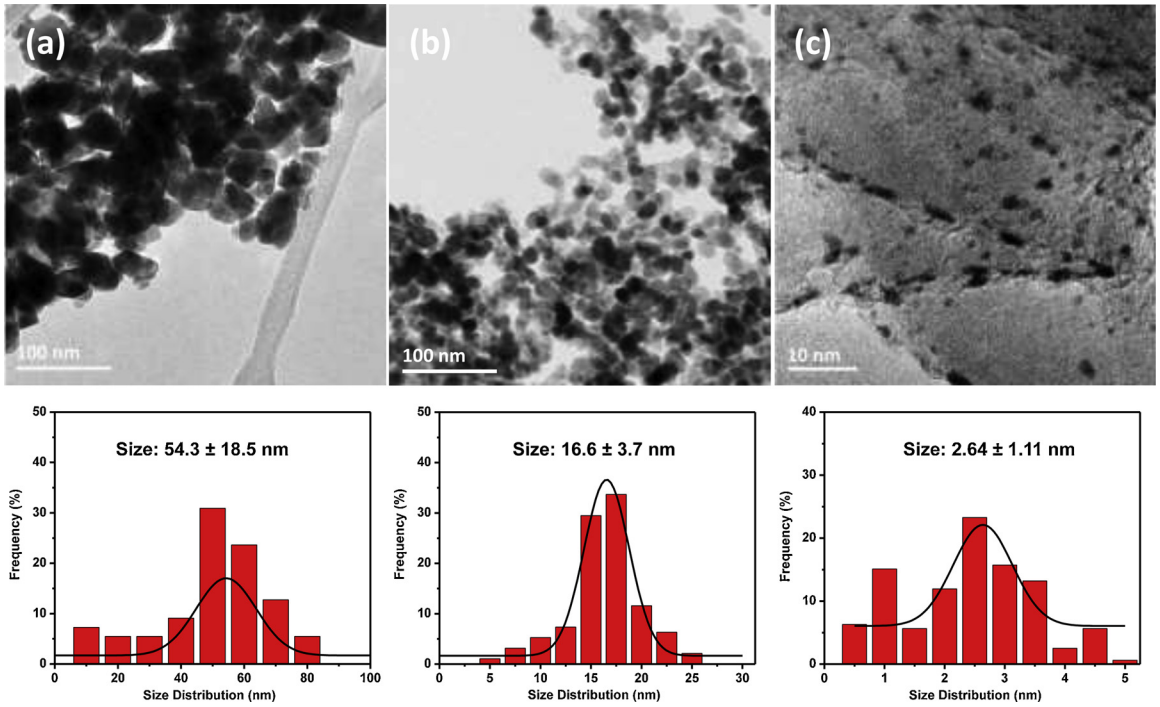

Fig. 1. TEM images of (a) lg-WO_3 NPs, (b) m-WO_3 NPs, and (c) 1% s-WO_3 NPs/graphite. The figures below each TEM images are the corresponding statistical counting of nanoparticle sizes (100 particles were used for counting). The average sizes of small, medium, and large WO_3 NPs are 2.64 ± 1.11 nm, 16.6 ± 3.7 nm, and 54.3 ± 18.5 nm, respectively.

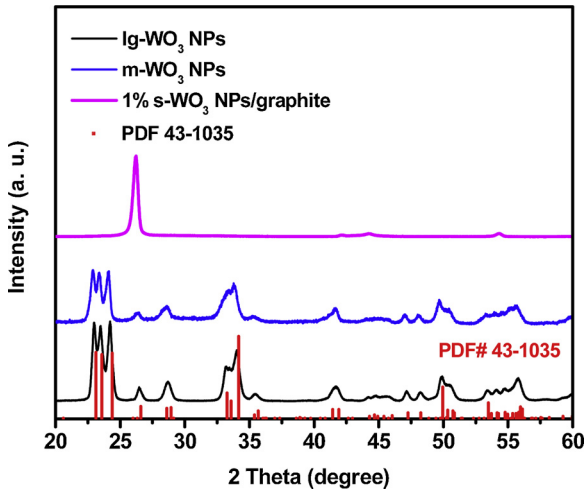

Fig. 2. X-ray diffraction patterns of lg-WO_3 NPs, m-WO_3 NPs, and 1% s-WO_3 NPs/graphite.

Table 1
Surface areas of different-sized WO_3 NPs calculated with average particle sizes obtained both from TEM images and N_2 adsorption.

Catalyst	TEM Surface Area (m^2/g)	BET Surface Area (m^2/g)
lg-WO_3	15.5	14.47
m-WO_3	50.5	56.31
s-WO_3	316	–

surface areas of different-sized WO_3 NPs, which are presented in Fig. 3b. Surface-specific/Areal formation rates of propylene exhibited a clear increasing trend with the decrease of particle size. Most notably, the areal propylene formation rate increased by two orders of magnitude from 1.62×10^{-4} mmol/m^2/h for lg-WO_3 NPs (54.3 nm) to 1.07×10^{-2} mmol/m^2/h for s-WO_3 NPs (2.64 nm). Given that the sizes of WO_3 NPs remained after catalysis (Fig. S2), we hypothesize that the WO_3 NPs must possess a drastically different composition of active sites as a function of particle size.

3.3. XPS studies of fresh and post-reaction catalysts

The difference in areal reaction rate as a function of WO_3 particle size is indicative of distinctly different surface structures for different-sized WO_3 NPs. Due to the high oxophilicity of tungsten, unsaturated W sites with a reduced electronic state will be readily oxidized upon exposure to ambient conditions. In order to capture the authentic surface structures, post-reaction catalysts were characterized by XPS without exposure to air. Fig. 4 shows the W 4f photoemission features of lg-WO_3 NPs, m-WO_3 NPs, and s-WO_3 NPs before and after reaction. The main photoemission peak of W $4f_{7/2}$ for all the three fresh catalysts was 35.5 eV, consistent with the feature of W^{6+} in bulk WO_3 [24,26]. A small portion of W^{5+} at 34.3 eV was observed on lg-WO_3 NPs and m-WO_3 NPs, suggesting their original surfaces were not completely saturated.

The photoemission features of post-reaction catalysts generally showed a higher portion of reduced W states, which was consistent with reported partial reduction of WO_3 during olefin metathesis reactions [27]. The higher proportion of reduced W states suggests an increase in the degree of surface unsaturation. For lg-WO_3 NPs and m-WO_3 NPs, the portion of W^{5+} slightly increased, while in the case of s-WO_3 NPs, the portion of W^{5+} increased dramatically with the emergence of W^{4+}. The degree of surface unsaturation can be described by the O/W surface atomic ratio (Fig. 4d). Based on stoichiometry, the atomic ratio of O to W of a saturated WO_3 surface should be 3. A decrease of the surface atomic ratio of O to W is indicative of an increase in the number of under-coordinated sites, as surface lattice oxygen is partially removed. Fig. 4d presents a decreasing trend of surface atomic ratio of O to W of post-reaction WO_3 NPs with a decrease of particle size. Specifically, the measured surface O/W atomic ratios for post-reaction lg-WO_3, m-WO_3, and s-WO_3 NPs were 2.97, 2.93, and 2.87, respectively. These data show that smaller WO_3 NPs have a higher degree of surface

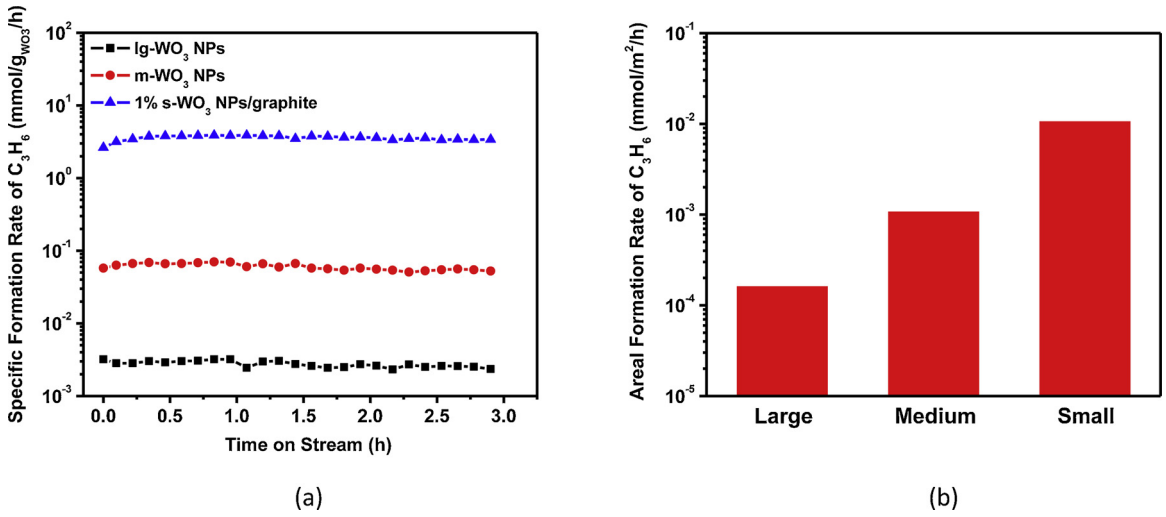

Fig. 3. Catalytic performance of lg-WO_3 NPs, m-WO_3 NPs, and 1% s-WO_3 NPs/graphite in terms of (a) propylene formation rates normalized by mass of WO_3, and (b) propylene formation rates normalized by exposed surface area of WO_3. Reaction conditions: 200 mg of catalyst was pretreated in He at 550 °C for 1 h before introducing the reactant mixture consisting of 10% ethylene and 10% trans-2-butene balanced with He with a flow rate of 100 ml/min.

unsaturation during catalysis. By correlating the degree of surface unsaturation of different-sized WO_3 NPs with the corresponding catalytic performance, the change in metathesis activity with the decrease of particle size can be rationalized by the increased degree of surface unsaturation.

3.4. Tuning the degree of surface unsaturation

Many synthetic protocols can be used to alter the degree of surface unsaturation of metal oxides. For instance, treating the catalysts in an inert gas or oxygen deficient atmosphere at a higher temperature can remove surface lattice oxygen atoms via thermal reduction, leading to an increase in the degree of surface unsaturation [28]. On the other hand, annealing unsaturated surfaces of WO_3 in air is able to saturate the surface with oxygen close to a stoichiometric ratio of O to W. Therefore, we employed different thermal treatments on freshly calcined samples prior to catalysis to control O/W surface ratios and thus gain further insight on the correlation between surface unsaturation and catalytic activity. Note that oxygen is used in industrial metathesis process for occasional coke burnoff, which also saturates the tungsten

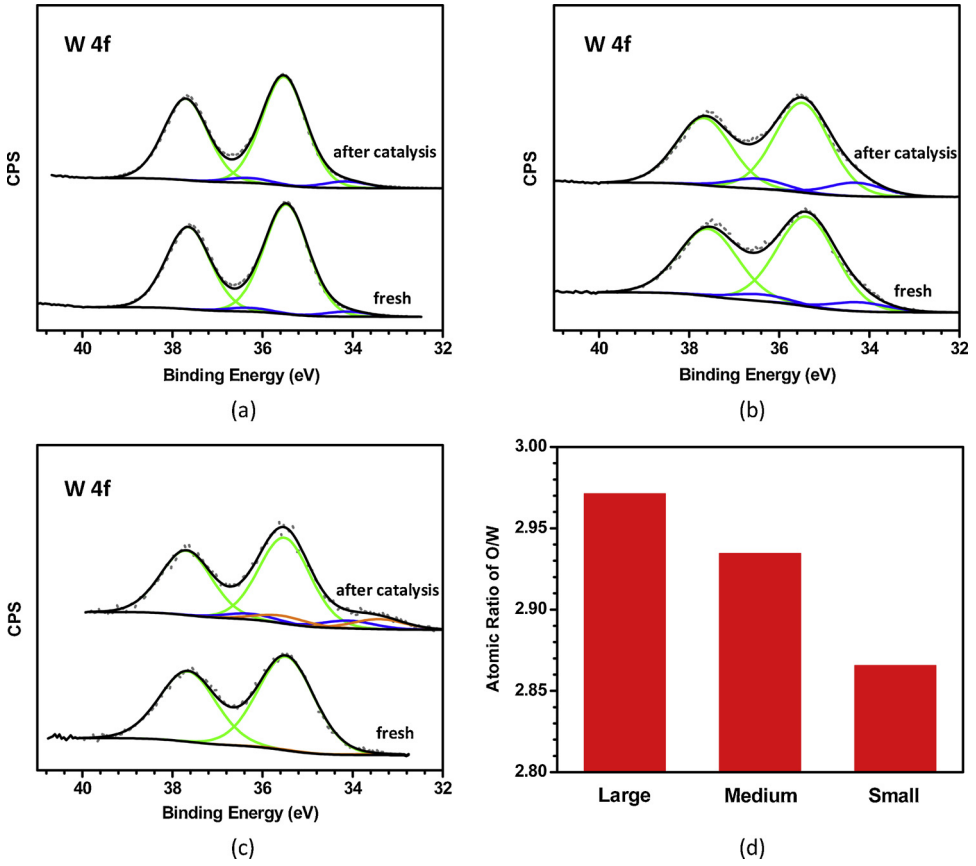

Fig. 4. Photoemission features of (a) lg-WO_3 NPs, (b) m-WO_3 NPs, and (c) s-WO_3 NPs before and after catalysis. (d) Calculated atomic ratios of O to W at near-surface region of different-sized WO_3 NPs after catalysis. In the peak fitting, the contributions of W^{6+}, W^{5+} and W^{4+} are fitted with green, blue, and orange curves, respectively (For interpretation of the references to colour in this figure legend, the reader is referred to the web version of this article).

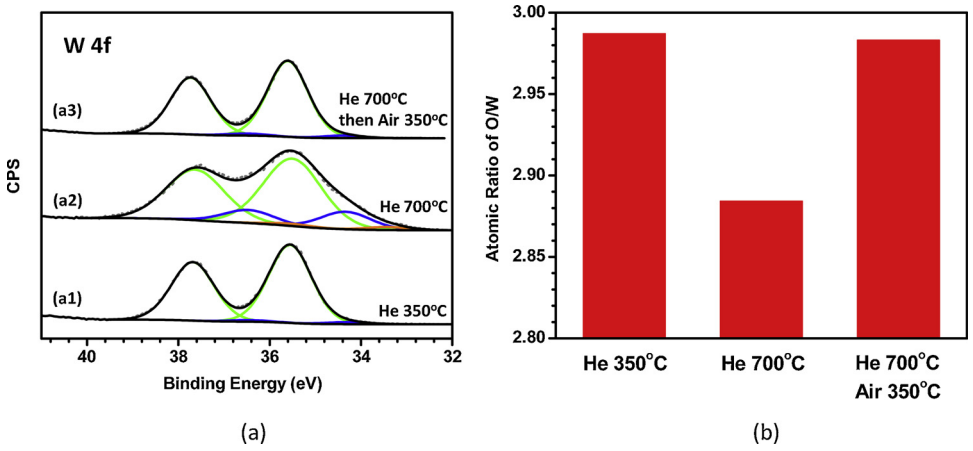

Fig. 5. (a) Photoemission features, peak fitting, and (b) calculated surface atomic ratios of O to W of l-WO_3 NPs under different treatment conditions. All spectra were taken on post-treatment catalysts without the exposure to ambient conditions. In the peak fitting, the contributions of W^{6+}, W^{5+} and W^{4+} are fitted with green, blue, and orange curves, respectively (For interpretation of the references to color in this figure legend, the reader is referred to the web version of this article).

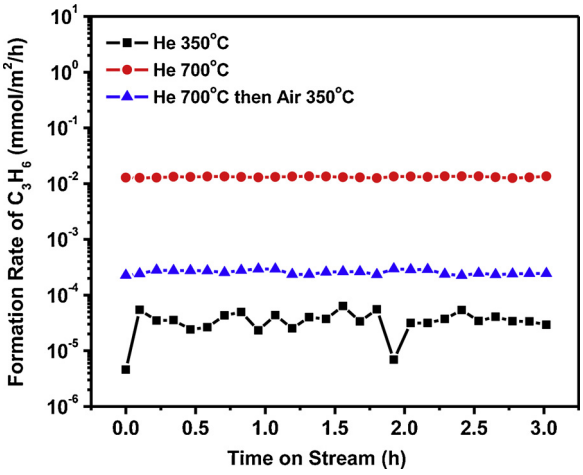

Fig. 6. Catalytic performances of lg-WO_3 NPs after different treatments. The catalysts were purged with He after treatments at 350 °C before a reactant mixture of 10% ethylene and 10% trans-2-butene balanced with He with a flow rate of 100 ml/min was introduced. Formation rates of propylene normalized by surface area are plotted as a function of time on stream.

sites. A subsequent treatment of inert gas or diluted hydrogen at a high temperature is typically applied in order to create an unsaturated W site again for increased metathesis activity.

Fig. 5a shows the air-free XPS results of the W 4f photoemission features of lg-WO_3 NPs after different treatment conditions. The W 4f photoemission feature of lg-WO_3 NPs after treatment in He at 350 °C was very similar to that of the fresh lg-WO_3 NPs (Figs. 5a1 and 4a), in which the majority of surface W atoms were in the +6 state at 35.4 eV [24]. Treatment in He at 700 °C dramatically changed the W 4f photoemission spectrum, clearly indicating the appearance of reduced W states as W^{5+} at 34.3 eV and W^{4+} at 33.4 eV (Fig. 5a2) [24]. A subsequent annealing in air at 350 °C of the catalyst treated in He at 700 °C restored the catalyst surface to a fully oxygen-saturated state (Fig. 5a3). Consistent with the photoemission spectra, the calculated surface atomic ratios of O to W also showed a decrease from 2.99 to 2.88 for the treatment in He at 700 °C, followed by an increase for the subsequent treatment in air at 350 °C (Fig. 5b). These results suggest that the degree of surface unsaturation can be tuned by annealing WO_3 NPs at different temperatures and gas atmosphere.

The catalytic performance of lg-WO_3 NPs was measured after the above treatments, as shown in Fig. 6. Treatment in He at 350 °C yielded a propylene formation rate of ~3.3×10^{-5} mmol/m^2/h, which increased by three orders of magnitude to 1.3×10^{-2} mmol/m^2/h after the treatment in He at 700 °C. We hypothesize that such a significant enhancement in cross-metathesis activity results from an increased degree of surface unsaturation after high-temperature annealing in an inert gas. The subsequent treatment in air at 350 °C increased surface oxygen saturation of the catalyst and resulted in the decrease of metathesis activity to 2.5×10^{-4} mmol/m^2/h. Notably, this formation rate of propylene did not decrease fully to the original level observed after the He treatment at 350 °C. This effect could result from weakly-bond oxygen atoms after air treatment at 350 °C that could be removed more easily during propylene metathesis compared with those strongly-bond oxygen atoms formed after calcination at 550 °C in air.

4. Summary

Different-sized WO_3 NPs show distinctly different surface-specific activities in the catalytic reactions of cross-metathesis of ethylene and trans-2-butene to propylene. The metathesis activity increases significantly with the decrease of particle size. Air-free XPS studies reveal that a smaller size of WO_3 NPs leads to a higher degree of surface unsaturation during catalysis, which is positively related to the cross-metathesis activity. Further investigation showed that the degree of surface unsaturation not only is related to the particle size, but can be tuned with different treatment conditions as well. This study revealed the essence of size effect of WO_3 NPs and established a correlation between catalytic activities of cross-metathesis and the degree of surface unsaturation. It also provided new insights and approaches in tuning catalytic performance via structural factors.

Acknowledgements

The authors acknowledge the financial support from Saudi Aramco through the MIT Energy Initiative Grant No. 6930839.

Appendix A. Supplementary data

Supplementary material related to this article can be found, in the online version, at doi:https://doi.org/10.1016/j.apcata.2019.04.019.

References

[1] J. Mol, J. Mol, Catal. A: Chem. 213 (2004) 39–45.
[2] S. Lwin, I.E. Wachs, ACS Catal. 4 (2014) 2505–2520.
[3] N. Gholampour, M. Yusubov, F. Verpoort, Catal. Rev. 58 (2016) 113–156.
[4] J. Wu, A. Ramanathan, A. Biancardi, A. Jystad, M. Caricato, Y. Hu, B. Subramaniam, ACS Catal. 8 (2018) 10437–10445.
[5] S. Lwin, Y. Li, A.I. Frenkel, I.E. Wachs, ACS Catal. 6 (2016) 3061–3071.
[6] W. Limsangkass, P. Praserthdam, S. Phatanasri, J. Panpranot, S. Chaemchuen, W. Jareewatchara, S.K.N. Ayudhya, K. Suriye, React. Kinet. Mech. Cat. 113 (2014) 225–240.
[7] W. Limsangkass, P. Praserthdam, S. Phatanasri, J. Panpranot, N. Poovarawan, W. Jareewatchara, S.K.N. Ayudhya, K. Suriye, Catal. Lett. 144 (2014) 1524–1529.
[8] J.-F. Wu, A. Ramanathan, W.K. Snavely, H. Zhu, A. Rokicki, B. Subramaniam, Appl. Catal. A. 528 (2016) 142–149.

[9] H. Balcar, J. Čejka, Coord. Chem. Rev. 257 (2013) 3107–3124.
[10] N. Poovarawan, K. Suriye, J. Panpranot, W. Limsangkass, F.J.S.C. Aires, P. Praserthdam, Catal. Lett. 145 (2015) 1868–1875.
[11] Q. Zhao, S.-L. Chen, J. Gao, C. Xu, Transition Met. Chem. 34 (2009) 621–627.
[12] Z. Cheng, C.S. Lo, ACS Catal. 5 (2014) 59–72.
[13] Y. Bouhoute, D. Grekov, K. Szeto, N. Merle, A. De Mallmann, F. Lefebvre, G. Raffa, I. Del Rosal, L. Maron, R. Gauvin, ACS Catal. 6 (2015) 1–18.
[14] S. Lwin, I.E. Wachs, ACS Catal. 7 (2016) 573–580.
[15] K. Ding, A. Gulec, A.M. Johnson, T.L. Drake, W. Wu, Y. Lin, E. Weitz, L.D. Marks, P.C. Stair, ACS Catal. 6 (2016) 5740–5746.
[16] S. Chaemchuen, S. Phatanasri, F. Verpoort, N. Sae-Ma, K. Suriye, Kinet. Catal. 53 (2012) 247–252.
[17] K. Gayapan, S. Sripinun, J. Panpranot, P. Praserthdam, S. Assabumrungrat, RSC Adv. 8 (2018) 28555–28568.
[18] S. Cao, F.F. Tao, Y. Tang, Y. Li, J. Yu, Chem. Soc. Rev. 45 (2016) 4747–4765.
[19] K.W. Kolasinski, Surface Science: Foundations of Catalysis and Nanoscience, 3rd ed., Wiley, 2012.
[20] G.A. Somorjai, Y. Li, Introduction to Surface Chemistry and Catalysis, 2nd ed., Wiley, 2010.
[21] S.T. Hunt, T. Nimmanwudipong, Y. Román-Leshkov, Angew. Chem. Int. Ed. 53 (2014) 5131–5136.
[22] R. Gao, N. Hu, Z. Yang, Q. Zhu, J. Chai, Y. Su, L. Zhang, Y. Zhang, Nanoscale Res. Lett. 8 (2013) 32.
[23] L. You, F. Yang, X. He, Y. Sun, G. Lu, Proceedings IMCS 2012, (2012), pp. 1081–1084.
[24] S.L. Wang, Y.L. Mak, S. Wang, J. Chai, F. Pan, M.L. Foo, W. Chen, K. Wu, G.Q. Xu, Langmuir 32 (2016) 13046–13053.
[25] J.C. Mol, K.J. Ivin, Olefin Metathesis and Metathesis Polymerization, 2nd ed., Elsevier Science Publishing Co Inc, 1997.
[26] W. Morales, M. Cason, O. Aina, N.R. de Tacconi, K. Rajeshwar, J. Am. Chem. Soc. 130 (2008) 6318–6319.
[27] J.G. Howell, Y.-P. Li, A.T. Bell, ACS Catal. 6 (2016) 7728–7738.
[28] D. Maiti, Y.A. Daza, M.M. Yung, J.N. Kuhn, V.R. Bhethanabotla, J. Mater. Chem. A 4 (2016) 5137–5148.